Hydrogenated Si–O–C nanoparticles: Synthesis, structure, and thermodynamic stability

Amir H. Tavakoli and Matthew M. Armentrout
Peter A Rock Thermochemistry Laboratory and NEAT ORU, University of California, Davis, California 95616, USA

Sabyasachi Sen
Department of Chemical Engineering and Materials Science, University of California, Davis, California 95616, USA

Alexandra Navrotsky[a)]
Peter A Rock Thermochemistry Laboratory and NEAT ORU, University of California, Davis, California 95616, USA; and Department of Chemical Engineering and Materials Science, University of California, Davis, California 95616, USA

(Received 15 September 2014; accepted 20 November 2014)

In the present work, for the first time, the inorganic Si-based materials lacking preexisting mixed bonds (O–Si–C, silicon in tetrahedral coordination bonded to both carbon and oxygen) have been successfully used as starting materials in a laser evaporation/condensation system for making hydrogenated silicon oxycarbide (Si–O–C–H) nanoparticles containing mixed bonds. The obtained materials are characterized by spectroscopic, microscopic, and calorimetric measurements. Thermodynamically stable 5–10 nm amorphous Si–O–C–H particles with a complex structure containing a combination of pure and mixed Si-based tetrahedral units (SiO_iC_{4-i}; i = 0–4), and a considerable amount of Si–OH and C–H bonds have been synthesized. The nanoparticles possess high surface areas (428–467 m^2/g), suggesting potential use in functionalities requiring high surface to volume ratios. In addition, making thermodynamically stable Si–O–C–H ceramics using a pathway different from the polymer route raises the likelihood of formation of similar carbon containing compounds in the planetary accretion and the Earth's interior.

I. INTRODUCTION

To satisfy the increasing global demand for (multi) functional silicon-based covalent ceramics, it is required to develop new products and technologies. The high temperature pyrolysis of organosilicon polymer precursors has been used for the synthesis of amorphous silicon oxycarbide (Si–O–C) and silicon carbonitride (Si–C–N) ceramics.[1–3] Polymer derived silicon-based ceramics have unique structures containing corner sharing Si-based tetrahedra and, in most cases, "free" carbon. In the case of Si–O–C ceramics, a fraction of the tetrahedral units consists of identical bonds (SiC_4 and SiO_4) and the remaining contains mixed bonds (SiO_iC_{4-i}; i = 1–3).[4–6] Similarly for most Si–C–N ceramics, the structure contains Si tetrahedra with both identical and mixed bonds (SiN_jC_{4-j}; j = 0–4).[7–9] Although the development of new Si-based ceramic products from polymer precursors has advantages such as the formation of tailored atomic structures and the capability of shaping polymers into a variety of forms, exploring alternative routes for making similar compositions/structures, particularly at nanoscale dimensions, is desirable as the chemistry and structure of polymer derived ceramics are dictated and therefore limited by the starting polymer. Along with the polymer approach, a variety of deposition techniques (e.g., CVD, sputtering, and PLD) for making Si–O–C and Si–C–N thin films have been used.[10–14] Although the synthesis of Si–O–C and Si–C–N nanoparticles using laser spray pyrolysis of Si-organic precursors has been reported,[15,16] the synthesis of nanoparticles using solely inorganic Si-based starting materials has not been documented to the best of our knowledge. Here, we present a straightforward technique for the synthesis of silicon oxycarbide nanoparticles. We selected the Si–O–C system mainly for two reasons. (i) Polymer derived Si–O–C compositions have been shown to be thermodynamically stable relative to the competitive crystalline components of SiO_2, SiC, and C,[17,18] implying the potential to form them by other pathways in both laboratory and natural settings, including planetary interiors and/or during planetary accretion. This possibility is supported if one can achieve the synthesis of similar Si–O–C materials through alternative methods in addition to the polymer route. (ii) A very recent

[a)]Address all correspondence to this author.
e-mail: anavrotsky@ucdavis.edu
DOI: 10.1557/jmr.2014.376

 © Materials Research Society 2015

https://doi.org/10.1557/jmr.2014.376 Published online by Cambridge University Press

report reveals outstanding gas sensing behavior of mesoporous Si–O–C ceramics.[19] Thus making Si–O–C nanoparticles with high surface area may not only improve the performance of the ceramic as a gas sensor but also be implemented for other applications such as batteries and catalysts.

II. EXPERIMENTAL PROCEDURES

A custom-made gas-phase condensation setup designed for laser evaporation of a solid target in a controlled atmosphere chamber (see Ref. 20 for details) was used for the synthesis. Two target compositions were used: (i) amorphous silicon monoxide (SiO_x; $x \approx 1$) pellets prepared by spark plasma sintering of SiO_x powders (Sigma-Aldrich, St. Louis, MO) at 1200 °C for 10 min under 100 MPa pressure; (ii) fused silica disks (Technical Glass Products, Painesville, OH). Prior to the vaporization, the synthesis chamber was evacuated below 9×10^{-3} Torr using an oil-free scroll pump and then filled to 10 Torr with 99.9% acetylene (C_2H_2) gas. The CW–CO_2 laser beam, focused on the target rotating at 6 rpm, was set at an operating power of 25 W throughout the evaporation time of ~30 min. Due to a slight pressure increase in the synthesis chamber during the synthesis process, possibly due to the formation of gaseous reaction byproducts, the chamber was evacuated and refilled with acetylene every 5 min. Deposits formed by condensation were collected on a stainless steel shim located 50 mm from the target. After synthesis, the as-deposited powders were scraped off the steel shim and stored.

X-ray diffraction (XRD) patterns were collected using a Bruker AXS D8 Advance diffractometer applying Cu K_α radiation (40 kV/40 mA). Chemical analysis was performed by Mikroanalytisches Labor Pascher applying combustion based techniques for hydrogen, oxygen, and carbon and inductively coupled plasma atomic emission spectroscopy (ICP-AES) for silicon. The morphology of the as-deposited powders was determined by transmission electron microscopy (TEM) using a JEOL JEM-2500SE instrument operated at 200 kV. For sample preparation, the particles were dispersed in ethanol and subsequently drop-cast on holey carbon films supported by TEM specimen grids. Selected area electron diffraction (SAED) was performed on particles reaching over holes to avoid electron diffraction intensity from the amorphous carbon support. Full adsorption/desorption isotherms of nitrogen at partial pressures $P/P^0 = 0$–1 (P^0 is the saturation pressure at −196 °C) were collected using a Micromeritics ASAP 2020 instrument. Surface area was measured applying the Brunauer Emmett Teller (BET) method. A Netzsch 449 TG/DSC instrument was used for the thermogravimetric (TG) analysis. The evolved gas was analyzed using a MKS Cirrus 2 mass spectrometer.

^{29}Si magic-angle-spinning nuclear magnetic resonance (MAS NMR) and ^{13}C(^{1}H) cross-polarization (CP) MAS NMR spectroscopic measurements were performed on each sample. ^{1}H MAS NMR measurements were performed on the sample obtained using the fused silica target. The ^{29}Si and ^{13}C NMR spectra were collected using a 4 mm Bruker CPMAS probe and a Bruker Avance solid-state spectrometer operating at a field strength of 11.7 T. Samples were loaded into a ZrO_2 rotor and spun at 10 kHz for ^{29}Si and ^{13}C(^{1}H) measurements. The single-pulse ^{29}Si NMR spectra were collected at a Larmor frequency of 99.3 MHz using a 60° tip angle (2.39 μs) and a recycle delay of 120 s. Approximately 1000 free induction decays (FIDs) were averaged and Fourier transformed to produce the final spectra. ^{29}Si chemical shifts were externally referenced to tetramethylsilane. ^{13}C(^{1}H)CPMAS measurements were collected at a Larmor frequency of 125.8 MHz for ^{13}C, using a 90° pulse of 2.75 μs, a ^{1}H spin-locking frequency of 38.5 kHz with a contact time of 2 ms, and a recycle delay of 5 s. FIDs were collected under a two-pulse-phase-modulated proton decoupling with a phase modulation angle of 15° and a pulse duration of 6.5 μs in the proton channel. Between 13,000 and 15,000 FIDs were averaged to obtain the spectra. ^{13}C chemical shifts were referenced to glycine. Single-pulse ^{1}H MAS NMR spectrum was collected at a Larmor frequency of 499.75 MHz using a 1.2 mm Agilent CPMAS probe and an Agilent VNMRS spectrometer equipped with an Oxford wide-bore magnet (11.7 T). The sample was spun at 55 kHz in a ZrO_2 rotor. A total of 160 FIDs were collected using a pulse tip angle of 45° (0.8 μs), recycle delay of 60 s, and chemical shift was referenced to adamantane.

High temperature oxidative drop solution calorimetry was used to determine the enthalpy of formation of the sample. This method is well developed[21–24] and has been applied previously to study Si–O–C ceramics.[17,18,25] Using this technique, 1–2 mg pellets were dropped from room temperature into molten sodium molybdate ($3Na_2O{\cdot}4MoO_3$) solvent at 802 °C in a custom built Tian-Calvet twin microcalorimeter[22,23] under an oxidizing atmosphere. The reaction rate of the pellet with solvent was accelerated and oxidizing conditions maintained by bubbling oxygen through the solvent at ~5 mL/min. The pellet dissolved in the solvent within an hour, and converted to cristobalite and CO_2 and H_2O gases evolved as a result of oxidation. To remove the evolved gases, the oxygen flow at 90 mL/min was used to continuously flush the headspace above the solvent inside the calorimeter. Multiple runs of 1–2 mg pellets were done to obtain appropriate statistics. The calorimeter was calibrated using the heat content of platinum pieces, as described earlier.[26–28]

https://doi.org/10.1557/jmr.2014.376 Published online by Cambridge University Press

III. RESULTS AND DISCUSSION

The XRD patterns of the as-obtained deposits are shown in Fig. 1. Except for a few weak peaks that can be readily assigned to SiC, no other peaks were detected, indicating that the deposited materials are mainly amorphous. The bright field TEM image taken from the deposits obtained using the fused silica target is shown in Fig. 2. The particles are nanometer sized with a narrow size distribution ranging from 5 to 10 nm and are highly agglomerated. Their SAED pattern, inset of Fig. 2, shows the halo rings commonly observed for amorphous materials. Thus, the TEM study confirms the formation of amorphous nanoparticles. Since no sign of crystalline SiC was detected by TEM, in contrast to the XRD patterns, we believe that crystalline SiC may not be a product of the primary evaporation/condensation process. In this connection, we observed that a thin layer of SiC forms on the target during the course of synthesis. We surmise that when the high-density laser beam hits the target, some SiC particles detach from the target surface, reach the steel shim, and contaminate the amorphous nanoparticles. We did not detect any crystalline phase by the TEM analysis because, most probably, large and relatively dense SiC particles were segregated during the TEM sample preparation and only the light fluffy amorphous deposits were dispersed in acetone and drop-cast on the TEM grid.

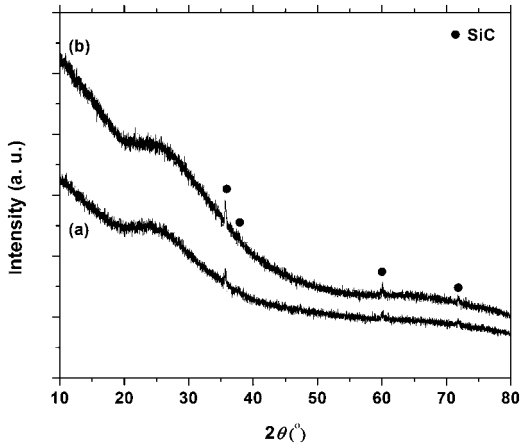


FIG. 1. XRD patterns of the samples obtained using SiO (a) and fused silica (b) targets.

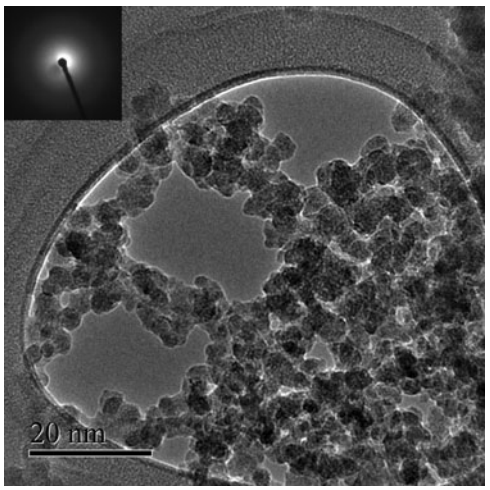


FIG. 2. Bright field transmission electron microscope (TEM) image taken from the deposits obtained using fused silica target. SAED pattern is shown in the inset of the figure.

The N_2 adsorption/desorption isotherms showed pronounced desorption hysteresis (Fig. 3), suggesting the existence of mesopores between particles. The BET surface areas (SAs) were 467 ± 2 and 428 ± 1 m^2/g for the amorphous nanoparticles obtained using silicon monoxide and fused silica targets, respectively. The amorphous nanoparticles obtained in this work have SAs almost three times greater than the mesoporous silicon oxycarbide ceramic for which good gas sensing behavior has been reported.[19] Thus, the new product introduced in this work may be an excellent candidate for use as a gas sensor.

The ^{29}Si MAS NMR spectra are shown in Fig. 4. Silicon in both samples exhibits a highly variable bonding environment. The strongest peak in these spectra in Fig. 4 corresponding to SiO_4 environments is characterized by chemical shifts of −100 and −107 ppm for the samples obtained using silicon monoxide and fused silica targets, respectively. Although the latter chemical shift is consistent with that observed in amorphous polymer-derived SiOC ceramics,[6] the peak at −100 ppm most likely corresponds to a Q^3-type SiO_4 environment with three bridging oxygen atoms and one terminating OH group. The second strongest peak near ~66 ppm in both ^{29}Si MAS NMR spectra corresponds to a SiO_3C unit with one nonbridging oxygen[29] or possibly a terminating OH group, suggesting a lesser degree of polymerization in these samples. These observations are consistent with

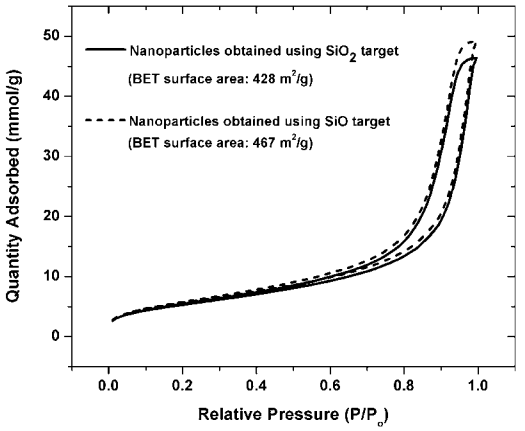


FIG. 3. Full N_2 adsorption/desorption isotherms measured on the as-obtained deposits after degassing at 400 °C.

https://doi.org/10.1557/jmr.2014.376 Published online by Cambridge University Press

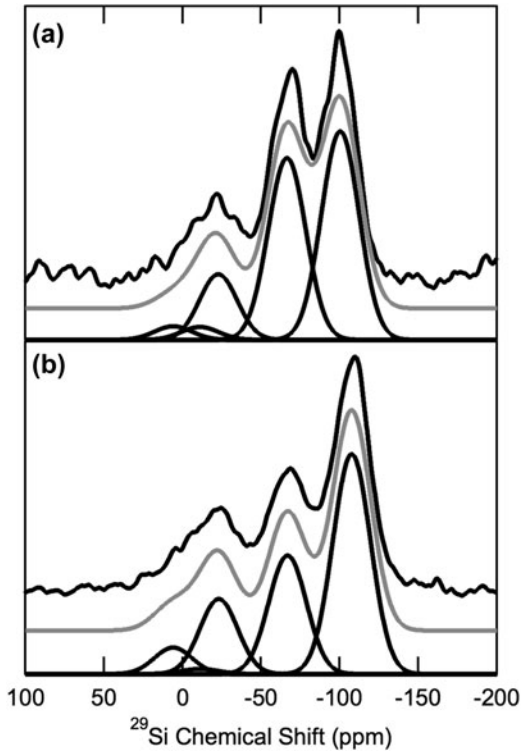


FIG. 4. ^{29}Si MAS NMR spectra samples obtained using SiO (a) and fused silica (b) targets. The raw spectra are shown on the top in black, fitted spectra in gray, and individual components in black on the bottom. The peaks at ~ −100, −66, −23, 6, and −11 ppm correspond to SiO_4, SiO_3C, SiO_2C_2, $SiOC_3$, and SiC_4, respectively.

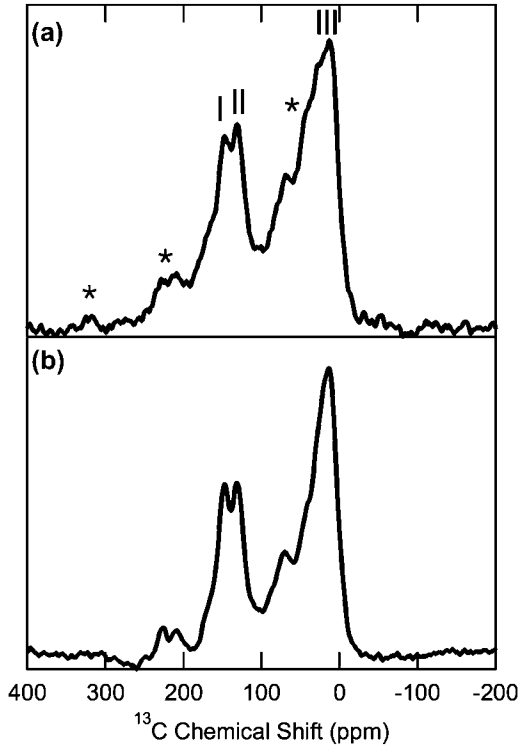


FIG. 5. ^{13}C CPMAS NMR of the samples obtained using SiO (a) and fused silica (b) targets. Peak I (~150 ppm) and Peak II (~130 ppm) correspond to sp^2 hybridized "free" carbon. The sidebands of these peaks are labeled with asterisks. Peak III (~15 ppm) corresponds to sp^3 hybridized carbon in the silica network.

TABLE I. Silicon site occupancies of each sample inferred from ^{29}Si MAS NMR measurements.

Sample	SiO_4	SiO_3C	SiO_2C_2	$SiOC_3$	SiC_4
Obtained from SiO_x	43.2	37.7	13.6	2.7	2.8
Obtained from fused silica	49.4	26.6	16.9	1.2	6.0

TABLE II. Elemental analysis of the Si–O–C–H sample.

Si	O	C	H
41.2 ± 0.3[a] (18.8)	40.0 ± 0.1 (32.0)	16.1 ± 0.1 (17.2)	2.50 ± 0.1 (32.0)

wt%, at.% in parentheses. Uncertainty is two standard deviations of the mean.

the high hydrogen content in these samples (see below). The remaining peaks for SiO_2C_2, $SiOC_3$, and SiC_4 units are located at −23, 6, and −11 ppm, respectively, as in Widgeon et al.[6] The relative abundances of each of these sites, as obtained from spectral line shape simulation (Fig. 1), are listed in Table I. Using the measured chemical composition of the sample obtained using the fused silica target (see Table II), we can estimate that ~90% of oxygen atoms are bridging. The nonbridging oxygen atoms are believed to be linked to hydrogen because, on the one hand, other than Si, C and O, H has been the only element available in the synthesis environment and, on the other hand, the surface water chemisorbed after exposing the obtained nanoparticles to air atmosphere can cause the formation of OH groups.

^{13}C(^{1}H) CPMAS NMR spectra are shown in Fig. 5. Three peaks are evident. The first two peaks at approximately −150 and −130 ppm correspond to sp^2 coordinated carbon as in Widgeon et al.[6] The third peak at −15 ppm corresponds to sp^3 coordinated carbon in the Si-based tetrahedral network. CPMAS NMR spectra being nonquantitative, the ratio of sp^2/sp^3 C cannot be estimated from these spectra.

The amorphous Si–O–C–H sample obtained using the fused silica target was used to check the thermodynamic stability. Its analyzed composition is given in Table II. To assign a chemical composition to the nanosample, the amounts of adsorbed surface water and crystalline SiC impurity need to be quantified. Using the TG analysis conducted from 25 to 1000 °C, a weight loss of 7 wt% was measured (Fig. 6). Evolved gas analysis done by a mass spectrometer throughout the TG measurement confirmed that only H_2O evolves, as no signal from the evolution of other gases like H_2, CH_4, CO, CO_2, or SiO was detected (Fig. 7). Thus, the whole mass loss is

https://doi.org/10.1557/jmr.2014.376 Published online by Cambridge University Press

attributed to water loss. Although the results of the XRD analysis indicate the existence of a small fraction of crystalline SiC, the ^{29}Si MAS NMR spectra do not show any indication of the crystallinity. Therefore, the amount of crystalline SiC cannot exceed a few mol% and such a small amount of the contamination may only affect the results of calorimetric measurements within their uncertainties. So, we disregarded the crystalline SiC phase amount in our calculations. Accordingly, the composition of the nano Si–O–C–H sample was determined to be $0.857Si_{0.22}O_{0.32}C_{0.20}H_{0.26}{\cdot}0.047H_2O(Si_{0.19}O_{0.32}C_{0.17}H_{0.32})$.

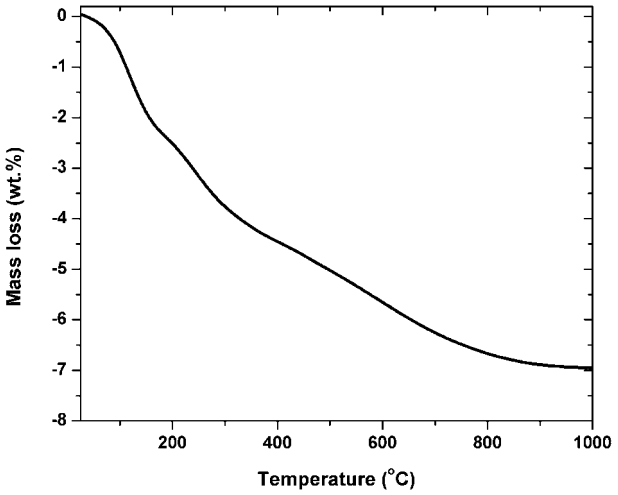


FIG. 6. TG measurement results of the nano Si–O–C–H sample obtained using the fused silica target indicating the weight loss as a function of temperature.

(This formula is given in the current format to be consistent in recalling the composition of the anhydrous Si–O–C–H phase throughout the manuscript.) When a Si–O–C–H pellet is dissolved in the solvent during the drop-solution calorimetric measurement, the oxidative dissolution reaction, represented by Eq. (1), has a corresponding enthalpy, which we call ΔH_{ds} of Si–O–C–H:

$$0.857Si_{0.22}O_{0.32}C_{0.20}H_{0.26}\cdot 0.047H_2O(25^{\circ}C) + 0.277O_2(802^{\circ}C) = 0.188SiO_2(802^{\circ}C) + 0.171CO_2(802^{\circ}C) + 0.158H_2O(802^{\circ}C) \quad . \quad (1)$$

The ΔH_{ds} measured for the nano Si–O–C–H sample equals -90.9 ± 3.0 kJ/g-atom. The ΔH_{ds} for the sample after correction for the surface water, through the thermodynamic cycle given in Table III, is -110.1 ± 3.1 kJ/g-atom. In our thermochemical calculations, the surface water was presumed to be physisorbed, as an attempt to measure the enthalpy of chemisorption failed, most probably due to the hydrophobic surface nature of the nanoparticles. Considering that the adsorption of water on hydrophobic surfaces, as are likely to exist in these samples, is expected to be weak, treating all the water as physisorbed water for correcting the experimentally obtained ΔH_{ds} is a good approximation. The corrected ΔH_{ds} value, combined with other known thermodynamic quantities, was used to calculate the oxidation enthalpy at 25 °C, ΔH_{ox}, the enthalpy of formation from the elements, $\Delta H_{f,\,elem}$, and the enthalpy

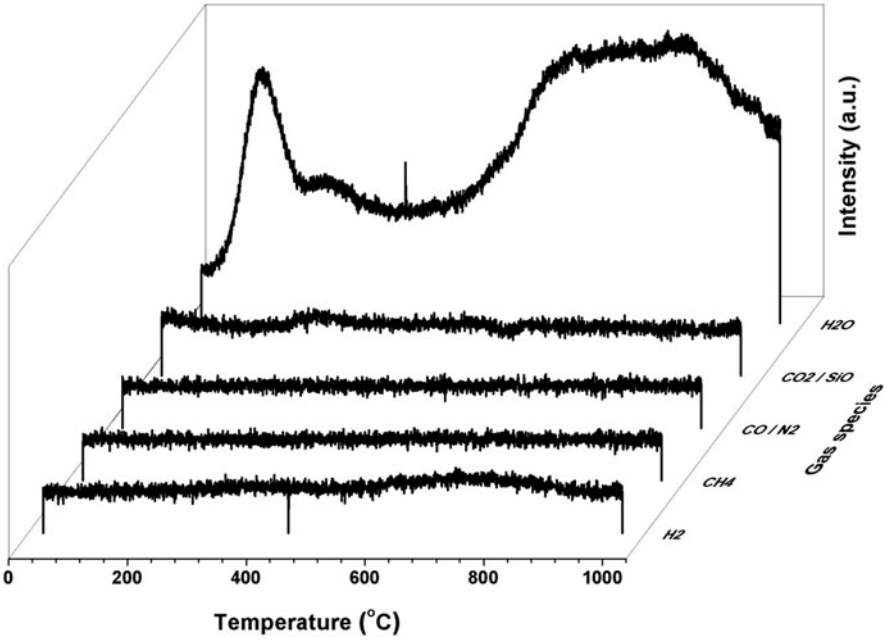


FIG. 7. Mass spectrometric analysis results of gas(es) evolved during the TG measurement. The detected signals corresponding to a number of potential gas species are plotted as a function of temperature.

https://doi.org/10.1557/jmr.2014.376 Published online by Cambridge University Press

TABLE III. Thermodynamic cycle for correcting the enthalpy of oxidative drop-solution for the surface water.

Reaction	Enthalpy (ΔH)
(1) 0.857 $Si_{0.22}O_{0.32}C_{0.20}H_{0.26}$·0.047 H_2O + 0.277 O_2 (802 °C) = 0.188 SiO_2 (802 °C) + 0.171 CO_2 (802 °C) + 0.158 H_2O (802 °C)	$\Delta H_1 = -90.9 \pm 3.0$ kJ/g-atom
(2) H_2O (liquid, 25 °C) → H_2O (gas, 802 °C)	$\Delta H_8 = 73.1$ kJ/mol[30]
(3) $Si_{0.22}O_{0.32}C_{0.20}H_{0.26}$ (25 °C) + 0.325 O_2 (802 °C) = 0.22 SiO_2 (802 °C) + 0.20 CO_2 (802 °C) + 0.13 H_2O (802 °C)	$\Delta H_9 = \Delta H_{ds,\ corrected}$
$\Delta H_9 = \Delta H_{ds,\ corrected} = (\Delta H_1 - 0.047\Delta H_2)/0.857 = -110.1 \pm 3.1$ kJ/g-atom	

TABLE IV. Thermodynamic cycles for the determination of (a) enthalpy of oxidation $\left(\Delta H^0_{ox}\right)$, (b) enthalpy of formation from the elements $\left(\Delta H^0_{f,\ elem}\right)$, and (c) enthalpy of formation from the components $\left(\Delta H^0_{f,\ comp}\right)$ at 25 °C for amorphous $Si_{0.22}O_{0.32}C_{0.20}H_{0.26}$.

Reaction	Enthalpy (ΔH)
a: Enthalpy of oxidation $\left(\Delta H^0_{ox}\right)$ at 25 °C	
(1) $Si_{0.22}O_{0.32}C_{0.20}H_{0.26}$ (solid, 25 °C) + 0.325 O_2 (gas, 802 °C) → 0.22 SiO_2 (cristobalite, 802 °C) + 0.20 CO_2 (gas, 802 °C) + 0.13 H_2O (gas, 802 °C)	$\Delta H_1 = \Delta H_{ds}$ (kJ/g-at.)
(2) SiO_2 (cristobalite, 25 °C) → SiO_2 (cristobalite, 802 °C)	$\Delta H_2 = 50.1$ kJ/mol[a, 30]
(3) H_2O (liquid, 25 °C) → H_2O (gas, 802 °C)	$\Delta H_3 = 73.1$ kJ/mol[30]
(4) O_2 (gas, 25 °C) → O_2 (gas, 802 °C)	$\Delta H_4 = 25.3$ kJ/mol[30]
(5) CO_2 (gas, 25 °C) → CO_2 (gas, 802 °C)	$\Delta H_5 = 37.5$ kJ/mol[30]
$Si_{0.22}O_{0.32}C_{0.20}H_{0.26}$ (solid) + 0.325 O_2 (gas) → 0.22 SiO_2 (cristobalite) + 0.20 CO_2 (gas) + 0.13 H_2O (liquid)	ΔH^0_{ox} (kJ/g-at.)
$\Delta H^0_{ox} = \Delta H_1 - 0.22\Delta H_2 - 0.13\Delta H_3 + 0.325\Delta H_4 - 0.20\Delta H_5$	
b: Enthalpy of formation from the elements $\left(\Delta H^0_{f,\ elem}\right)$ at 25 °C	
(1) $Si_{0.22}O_{0.32}C_{0.20}H_{0.26}$ (solid) + 0.325 O_2 (gas) → 0.22 SiO_2 (cristobalite) + 0.20 CO_2 (gas) + 0.13 H_2O (liquid)	$\Delta H_1 = \Delta H^0_{ox}$ (kJ/g-at.)
(2) Si (solid) + O_2 (gas) → SiO_2 (cristobalite)	$\Delta H_2 = -908.4 \pm 2.1$ kJ/mol[31]
(3) H_2 (gas) + 1/2 O_2 (gas) → H_2O (liquid)	$\Delta H_3 = -285.8 \pm 0.1$ kJ/mol[31]
(4) C (solid) + O_2 (gas) → CO_2 (gas)	$\Delta H_4 = -393.5 \pm 0.1$ kJ/mol[31]
0.22 Si (solid) + 0.16 O_2 (gas) + 0.20 C (solid) + 0.13 H_2 (gas) → $Si_{0.22}O_{0.32}C_{0.20}H_{0.26}$ (solid)	$\Delta H^0_{f,\ elem}$ (kJ/g-at.)
$\Delta H^0_{f,\ elem} = -\Delta H_1 + 0.22\Delta H_2 + 0.13\Delta H_3 + 0.20\Delta H_4$	
c: Enthalpy of formation from the components $\left(\Delta H^0_{f,\ comp}\right)$ at 25 °C	
(1) 0.22 Si (solid) + 0.16 O_2 (gas) + 0.20 C (solid) + 0.13 H_2 (gas) → $Si_{0.22}O_{0.32}C_{0.20}H_{0.26}$ (solid)	$\Delta H_1 = \Delta H^0_{f,\ elem}$ (kJ/g-at.)
(2) Si (solid) + C (solid) → SiC (solid)	$\Delta H_2 = -73.2 \pm 6.3$ kJ/mol[b, 30]
(3) Si (solid) + O_2 (gas) → SiO_2 (cristobalite)	$\Delta H_3 = -908.4 \pm 2.1$ kJ/mol[31]
0.06 SiC (solid) + 0.16 SiO_2 (cristobalite) + 0.14 C (solid) + 0.13 H_2 (gas) → $Si_{0.22}O_{0.32}C_{0.20}H_{0.26}$ (solid)	$\Delta H^0_{f,\ comp}$ (kJ/g-at.)
$\Delta H^0_{f,\ comp} = \Delta H_1 - 0.06\Delta H_2 - 0.16\Delta H_3$	

[a]Low cristobalite at 25 °C, high cristobalite at 802 °C.
[b]Enthalpy of formation of β-SiC.

TABLE V. Enthalpy of oxidative drop-solution at 802 °C corrected for the surface water and SiC impurity ($\Delta H_{ds,\ corrected}$), enthalpy of oxidation at 25 °C (ΔH_{ox}), enthalpy of formation from elements at 25 °C ($\Delta H_{f,\ elem}$), and enthalpy of formation from components SiO_2, SiC, C, and H_2 at 25 °C ($\Delta H_{f,\ comp}$) for the amorphous nano S–O–C–H sample.

$Si_aO_bC_cH_d$ ($a + b + c + d = 1$)							
a	b	c	d	$\Delta H_{ds,\ corrected}$ (kJ/g-atom)	ΔH_{ox} (kJ/g-atom)	$\Delta H_{f,\ elem}$ (kJ/g-atom)	$\Delta H_{f,\ comp}$ (kJ/g-atom)
0.22	0.32	0.20	0.26	-110.1 ± 3.1 (6)[a]	-129.9 ± 3.1	-185.8 ± 3.1	-36.1 ± 3.2

[a]Uncertainty is two standard deviations of the mean. The number inside the parentheses is the number of experiments.

of formation from components SiO_2, SiC, C, and H_2, $\Delta H_{f,\ comp}$, through the thermodynamic cycles given in Table IV. The obtained ΔH_{ox}, $\Delta H_{f,\ elem}$, and $\Delta H_{f,\ comp}$ values, listed in Table V, are -129.9 ± 3.1, -185.8 ± 3.1, and -36.1 ± 3.2 kJ/g-atom, respectively, indicating that the amorphous nano Si–O–C–H sample is energetically more stable than a mixture of the thermodynamically most stable crystalline elemental and binary components. It is notable that our data sensitivity analysis assuming 5 mol% SiC contamination indicated that the enthalpy of formation changes only for ~2.5 kJ/g-atom, which is within the uncertainty of our measurements as expected. Since the sp^3-bonded Si–O–C network is amorphous and disordered, one expects that the sample is higher in

https://doi.org/10.1557/jmr.2014.376 Published online by Cambridge University Press

entropy than the mixture of crystalline components. Accordingly, the negative enthalpy of formation coupled with the expected positive entropy of formation from these components ensures a negative Gibbs free energy of formation, confirming thermodynamic stability.

In the following, the structural and energetic impact of hydrogen are addressed, as the sample contains, perhaps unexpectedly, a considerable amount of H (32 at.%). Even after correcting the composition for water, as explained above, the H content of the anhydrous nanosample is still very high (26 at.%), indicating that only a small fraction of the measured H is bonded to the surfaces as physisorbed water. To confirm the chemical environment of H in the structure, a high-resolution ^{1}H MAS NMR spectrum of the nano Si–O–C–H sample, obtained using the fused silica target, was collected at very high spinning speed (55 kHz) (Fig. 8). Three dominant peaks are present in this spectrum at 1.0, 4.2, and 6.7 ppm. The resonances at 1.0 and 6.7 ppm are readily identifiable as C–H bonds with sp^3 and sp^2 carbon, respectively.[32,33] The peak at 4.2 ppm can correspond to either physisorbed water or Si–OH, as in El Kortobi et al.,[16] in agreement with our ^{29}Si MAS NMR measurements and the previously reported ^{1}H MAS NMR spectroscopic results on Si–O–C glasses,[34] suggesting the existence of Si–OH. The origin of H in the Si–OH groups could be either chemisorbed water or acetylene (H–C≡C–H) gas used as a carbon source for the synthesis. Although the formation of Si–OH groups through the dissociation of water is easily understandable, the reaction mechanism through which Si–OH groups possibly form by interacting the silicon source and acetylene is unclear. The origin of H forming C–H bonds is believed to be only acetylene gas, as the triple C≡C bonds in acetylene are extremely unstable and easily cleave during the synthesis but the single C–H bonds could remain on the surface or within the structure of the nanoparticles. To estimate the energetic role of hydrogen, we consider the formation reaction of the anhydrous Si–O–C nanoparticles containing H functional groups from a H-free bulk Si–O–C with a similar composition as the nanoparticles and H_2 gas, as follows:

$$Si_{0.30}O_{0.43}C_{0.27} + 0.175H_2 \rightarrow Si_{0.30}O_{0.43}C_{0.27} \cdot 0.175H_2 \quad . \tag{2}$$

Although the $\Delta H_{f,\ comp}$ of the H-free composition in Eq. (2) is not known, the $\Delta H_{f,\ comp}$ value for a similar composition ($Si_{0.31}O_{0.47}C_{0.22}$) has been measured ($\Delta H_{f,\ comp} = -9.9 \pm 2.0$ kJ/g-atom).[35] Assuming that $\Delta H_{f,\ comp}$ values for these two similar compositions $Si_{0.30}O_{0.43}C_{0.27}$ and $Si_{0.31}O_{0.47}C_{0.22}$ are equal, the enthalpy of formation of the anhydrous Si–O–H–C nanoparticles according to Eq. (2) equals $\Delta H_f = \Delta H_{f,\ comp}$ ($Si_{0.30}O_{0.43}C_{0.27}\cdot 0.175H_2$) – $\Delta H_{f,\ comp}$ ($Si_{0.30}O_{0.43}C_{0.27}$) $= -38.8 \pm 4.3$ kJ/g-atom of the Si–O–C composition (-221.7 ± 24.5 kJ/mol of H_2). (The enthalpy value was taken from Table V.) The strongly exothermic enthalpy obtained for reaction (2) suggests that, despite the unfavorable surface enthalpy due to the high surface area of the nano sample, the negative enthalpy originating from the functional H atoms is large enough to make the formation of hydrogenated nanoparticles energetically favorable relative to bulk hydrogen-free material. Similar stabilization driven by the surface functional groups has been suggested recently for onion-like carbon and diamond nanoparticles.[36,37]

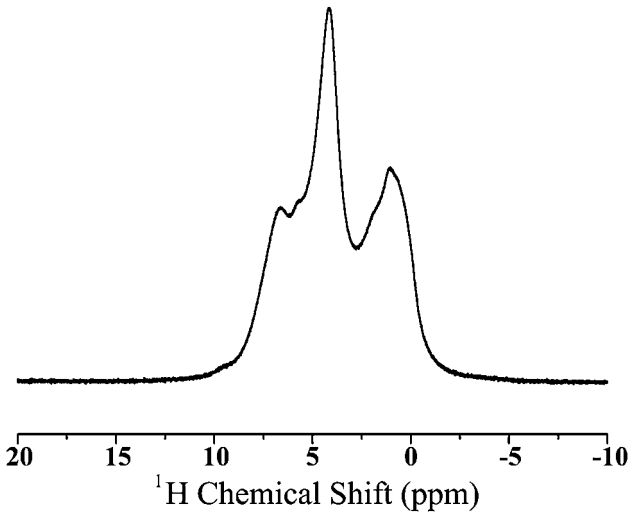


FIG. 8. ^{1}H MAS NMR spectrum of the nano Si–O–H–C sample obtained using the fused silica target. Dominant peaks are evident at 1.0, 4.2, and 6.7 ppm.

IV. CONCLUSIONS AND IMPLICATIONS

A reactive laser evaporation technique was applied to make Si–O–C nanoparticles without using Si-organic precursors. The technique itself is extremely versatile and can be applied for the synthesis of other complex covalent ceramics such as Si–C–N and B–C–N compounds. The obtained 5–10 nm amorphous nanoparticles contain mixed bonds (O–Si–C) and a significant amount of H bonded to C and to O. The origin of H is mainly from the reactive gas (C_2H_2) used for the synthesis and partly due to the surface water. The hydrogenated nanoparticles are thermodynamically more stable than the thermodynamically most stable components SiO_2, SiC, C, and H_2. The nanoparticles are also energetically stabilized relative to a bulk polymer derived SiOC ceramic of similar composition, implying that the stabilizing effect of hydrogenation is greater than the destabilization caused by a high surface to volume ratio. The Si–O–C–H nanoparticles are expected to show

https://doi.org/10.1557/jmr.2014.376 Published online by Cambridge University Press

promising functional properties, particularly when having a high surface area is desirable. The ability to synthesize SiOC materials with mixed bonding by a direct deposition route, without recourse to pyrolysis of organometallic polymers, is further evidence of their intrinsic stability as confirmed by calorimetric measurements. The laser evaporation/condensation route is much closer to the possible synthesis pathways in planetary condensation and these observations further support our earlier suggestion[29] that such SiOC materials could form in geologic and planetary environments.

ACKNOWLEDGMENTS

We thank Jorgen Rufner and Dana Reusser for their assistance in TEM and mass spectrometric measurements. We acknowledge financial supports by the National Science Foundation, grant DMR-124077 for salary support and materials science aspects of this work and by the Deep Carbon Observatory funded by the Sloan Foundation for inspiring us to consider the geologic and planetary relevance of these studies.

REFERENCES

1. E. Kroke, Y.L. Li, C. Konetschny, E. Lecomte, C. Fasel, and R. Riedel: Silazane derived ceramics and related materials. *Mater. Sci. Eng., R* **26**, 97 (2000).
2. P. Colombo, G. Mera, R. Riedel, and G.D. Soraru: Polymer-derived ceramics: 40 years of research and innovation in advanced ceramics. *J. Am. Ceram. Soc.* **93**, 1805 (2010).
3. G. Mera, A. Navrotsky, S. Sen, H.J. Kleebe, and R. Riedel: Polymer-derived SiCN and SiOC ceramics - Structure and energetics at the nanoscale. *J. Mater. Chem. A* **1**, 3826 (2013).
4. G.M. Renlund, S. Prochazka, and R.H. Doremus: Silicon oxycarbide glasses. 2. Structure and properties. *J. Mater. Res.* **6**, 2723 (1991).
5. A. Saha, R. Raj, and D.L. Williamson: A model for the nanodomains in polymer-derived SiCO. *J. Am. Ceram. Soc.* **89**, 2188 (2006).
6. S.J. Widgeon, S. Sen, G. Mera, E. Ionescu, R. Riedel, and A. Navrotsky: Si-29 and C-13 solid-state NMR spectroscopic study of nanometer-scale structure and mass fractal characteristics of amorphous polymer derived silicon oxycarbide ceramics. *Chem. Mater.* **22**, 6221 (2010).
7. J. Dixmier, R. Bellissent, D. Bahloul, and P. Goursat: Neutron-diffraction study of the amorphous phase-structure in silicon carbonitride ceramics obtained by pyrolysis of a polyvinylsilazane. *J. Eur. Ceram. Soc.* **13**, 293 (1994).
8. J. Seitz, J. Bill, N. Egger, and F. Aldinger: Structural investigations of Si/C/N-ceramics from polysilazane precursors by nuclear magnetic resonance. *J. Eur. Ceram. Soc.* **16**, 885 (1996).
9. J. Haug, P. Lamparter, M. Weinmann, and F. Aldinger: Diffraction study on the atomic structure and phase separation of amorphous ceramics in the Si-(B)-C-N system. 1. Si-C-N ceramics. *Chem. Mater.* **16**, 72 (2004).
10. C.S. Yang, K.S. Oh, J.Y. Ryu, D.C. Kim, S.Y. Jing, C.K. Choi, H.J. Lee, S.H. Um, and H.Y. Chang: A study on the formation and characteristics of the Si–O–C–H composite thin films with low dielectric constant for advanced semiconductor devices. *Thin Solid Films* **390**, 113 (2001).
11. H.J. Lee, K.S. Oh, and C.K. Choi: The mechanical properties of the SiOC(–H) composite thin films with a low dielectric constant. *Surf. Coat. Technol.* **17**, 296 (2003).
12. C.B. Wanga, T. Gotob, R. Tub, and L.M. Zhang: Preparation of silicon oxycarbide films by laser ablation of SiO/3C–SiC multi-component targets. *Appl. Surf. Sci.* **257**, 1703 (2010).
13. Z. Gong, E.G. Wang, G.C. Xu, and Y. Chen: Influence of deposition condition and hydrogen on amorphous-to-polycrystalline SiCN films. *Thin Solid Films* **348**, 114 (1999).
14. N. Park, S.H. Kim, and G.Y. Sung: Amorphous silicon carbon nitride films grown by the pulsed laser deposition of a SiC-Si_3N_4 mixed target. *ETRI J.* **26**, 257 (2004).
15. K.E. Gonsalves, P.R. Strutt, T.D. Xiao, and P.G. Klemens: Synthesis of Si(C, N) nanoparticles by rapid laser polycondensation/crosslinking reactions of an organosilazane precursor. *J. Mater. Sci.* **27**, 3231 (1992).
16. Y.El. Kortobi, J. d'Espinose de la Caillerie, and A. Legrand: Local composition of silicon oxycarbides obtained by laser spray pyrolysis. *Chem. Mater.* **9**, 632 (1997).
17. T. Varga, A. Navrotsky, J.L. Moats, R.M. Morcos, F. Poli, K. Muller, A. Sahay, and R. Raj: Thermodynamically stable $Si_xO_yC_z$ polymer-like amorphous ceramics. *J. Am. Ceram. Soc.* **90**, 3213 (2007).
18. R.M. Morcos, A. Navrotsky, T. Varga, Y. Blum, D. Ahn, F. Poli, K. Muller, and R. Raj: Energetics of $Si_xO_yC_z$ polymer-derived ceramics prepared under varying conditions. *J. Am. Ceram. Soc.* **91**, 2969 (2008).
19. A. Karakuscu, A. Ponzoni, P.R. Aravind, G. Sberveglieri, and G.D. Soraru: Gas sensing behavior of mesoporous SiOC glasses. *J. Am. Ceram. Soc.* **96**, 2366 (2013).
20. H. Eilers and B.M. Tissue: Synthesis of nanophase ZnO, EU_2O_3, and ZrO_2 by gas-phase condensation with CW-CO_2 laser-heating. *Mater. Lett.* **24**, 261 (1995).
21. J.M. McHale, G.R. Kowach, A. Navrotsky, and F.J. DiSalvo: Thermochemistry of metal nitrides in the Ca/Zn/N system. *Chem. -Eur. J.* **2**, 1514 (1996).
22. A. Navrotsky: Progress and new directions in high-temperature calorimetry. *Phys. Chem. Miner.* **2**, 89 (1977).
23. A. Navrotsky: Progress and new directions in high-temperature calorimetry. *Phys. Chem. Miner.* **24**, 222 (1997).
24. A. Navrotsky: Thermochemical studies of nitrides and oxynitrides by oxidative oxide melt calorimetry. *J. Alloys Compd.* **321**, 300 (2001).
25. A.H. Tavakoli, M.M. Armentrout, M. Narisawa, S. Sen, and A. Navrotsky: White Si-O-C ceramic: Structure and thermodynamic stability. *J. Am. Ceram. Soc.*, in press (DOI:10.1111/jace.13233).
26. J.J. Liang, L. Topor, A. Navrotsky, and M. Mitomo: Silicon nitride: Enthalpy of formation of the alpha- and beta-polymorphs and the effect of C and O impurities. *J. Mater. Res.* **14**, 1959 (1999).
27. J.J. Liang, A. Navrotsky, V.J. Leppert, M.J. Paskowitz, S.H. Risbud, T. Ludwig, H.J. Seifert, F. Aldinger, and M. Mitomo: Thermochemistry of $Si_{6-Z}Al_zO_zN_{8-Z}$ ($Z = 0$ to 3.6) materials. *J. Mater. Res.* **14**, 4630 (1999).
28. Y.H. Zhang, A. Navrotsky, and T. Sekine: Energetics of cubic Si_3N_4. *J. Mater. Res.* **21**, 41 (2006).
29. S. Sen, S.J. Widgeon, A. Navrotsky, G. Mera, A. Tavakoli, E. Ionescu, and R. Riedel: Carbon substitution for oxygen in silicates in planetary interiors. *Proc. Natl. Acad. Sci.* **110**, 15904 (2013).
30. C. Bale, P. Chartrand, S.A. Degterov, G. Eriksson, K. Hack, R. Ben Mahfoud, J. Melancon, A.D. Pelton, and S. Petersen: Factsage thermochemical software and databases. In *Calphad-Computer Coupling of Phase Diagrams and Thermochemistry*, Vol. **26**. (Computer Coupling of Phase Diagrams and Thermochemistry, 2002); pp. 189–228.

https://doi.org/10.1557/jmr.2014.376 Published online by Cambridge University Press

31. R.A. Robie and B.S. Hemingway: Thermodynamic properties of minerals and related substances at 298.15 K and 1 bar (105 Pascals) pressure and at higher temperatures. In *U. S. Geological Survey Bulletin 2131*. (United States Government Printing Office, Washington, DC, 1995).
32. R.M. Silverstein, G.C. Bassler, and T.C. Morrill: *Spectrometric Identification of Organic Compounds*, 5th ed. (Wiley, New York, NY, 1991).
33. S. Widgeon, G. Mera, Y. Gao, S. Sen, A. Navrotsky, and R. Riedel: Effect of precursor on speciation and nanostructure of SiBCN polymer-derived ceramics. *J. Am. Ceram. Soc.* **96**, 1651 (2013).
34. H. Bréquel, J. Parmentier, S. Walter, R. Badheka, G. Trimmel, S. Masse, J. Latournerie, P. Dempsey, C. Turquat, A. Desmartin-Chomel, L. Le Neindre-Prum, U.A. Jayasooriya, D. Hourlier, H-J. Kleebe, G.D. Sorarù, S. Enzo, and F. Babonneau: Systematic structural characterization of the high-temperature behavior of nearly stoichiometric silicon oxycarbide glasses. *Chem. Mater.* **16**, 2585 (2004).
35. A.H. Tavakoli, R. Campostrini, C. Gervais, F. Babonneau, J. Bill, G.D. Soraru, and A. Navrotsky: Energetics and structure of polymer-derived Si-(B-)O-C glasses: Effect of the boron content and pyrolysis temperature. *J. Am. Ceram. Soc.* **97**, 303 (2014).
36. G.C.C. Costa, J.K. McDonough, Y. Gogotsi, and A. Navrotsky: Thermochemistry of onion like carbons. *Carbon* **69**, 490 (2014).
37. G.C.C. Gustavo, O. Shenderova, V. Mochalin, Y. Gogotsi, and A. Navrotsky: Thermochemistry of nanodiamond terminated by oxygen containing functional groups. *Carbon* **80**, 544 (2014).

https://doi.org/10.1557/jmr.2014.376 Published online by Cambridge University Press